The Impact of Oceanic Near-Inertial Waves on Climate

MARKUS JOCHUM

Niels Bohr Institute, University of Copenhagen, Copenhagen, Denmark

BRUCE P. BRIEGLEB, GOKHAN DANABASOGLU, WILLIAM G. LARGE, AND NANCY J. NORTON

National Center for Atmospheric Research, Boulder, Colorado*

STEVEN R. JAYNE

Woods Hole Oceanographic Institution, Woods Hole, Massachusetts

MATTHEW H. ALFORD

Applied Physics Laboratory, Seattle, Washington

FRANK O. BRYAN

National Center for Atmospheric Research, Boulder, Colorado*

(Manuscript received 4 April 2012, in final form 8 October 2012)

ABSTRACT

The Community Climate System Model, version 4 (CCSM4) is used to assess the climate impact of wind-generated near-inertial waves (NIWs). Even with high-frequency coupling, CCSM4 underestimates the strength of NIWs, so that a parameterization for NIWs is developed and included into CCSM4. Numerous assumptions enter this parameterization, the core of which is that the NIW velocity signal is detected during the model integration, and amplified in the shear computation of the ocean surface boundary layer module. It is found that NIWs deepen the ocean mixed layer by up to 30%, but they contribute little to the ventilation and mixing of the ocean below the thermocline. However, the deepening of the tropical mixed layer by NIWs leads to a change in tropical sea surface temperature and precipitation. Atmospheric teleconnections then change the global sea level pressure fields so that the midlatitude westerlies become weaker. Unfortunately, the magnitude of the real air-sea flux of NIW energy is poorly constrained by observations; this makes the quantitative assessment of their climate impact rather uncertain. Thus, a major result of the present study is that because of its importance for global climate the uncertainty in the observed tropical NIW energy has to be reduced.

1. Introduction

Over the last decade increases in computer power have been large enough to make it possible for scientists to routinely integrate global general circulation models (GCMs) of the earth's climate for hundreds and thousands of years (e.g., Wittenberg 2009). When combined with recent claims that even past climates like glacial inceptions can be represented with GCMs (Jochum et al. 2012), it appears possible to simulate the evolution of climate over the span of human civilization or further (Liu et al. 2009). Over these time scales, though, it would appear to be necessary that GCMs are energetically consistent so that they contain no artificial energy sources or sinks.

It is current practice in the ocean component of GCMs (OGCMs) to present small-scale turbulence as constant diapycnal diffusivity. This diffusivity is a source of

* The National Center for Atmospheric Research is sponsored by the National Science Foundation.

Corresponding author address: Markus Jochum, Niels Bohr Institute, University of Copenhagen, Juliane Maries Vej 30, 2100 Copenhagen, Denmark.
E-mail: mjochum@nbi.dk

DOI: 10.1175/JCLI-D-12-00181.1

mechanical energy that lifts heavy bottom waters across the thermocline to the surface of the oceans (e.g., Munk and Wunsch 1998), and it is currently independent of the environmental conditions. Similarily, friction and parameterized baroclinic instability are sinks of mechanical energy in an OGCM, whereas in the real ocean some of this energy would be used for diabatic mixing and an increase in potential energy (Tandon and Garrett (1996). Thus, in GCMs mechanical energy is currently added and removed without being accounted for or being tied to real physical processes. Instead, the strength of the energy sources and sinks is manipulated to optimize the solution (i.e., Danabasoglu and Marshall 2007; Jochum et al. 2008).

One goal of current OGCM development is therefore to replace a constant background diffusivity with a diffusivity that is determined from the parameterized contributions of the different relevant processes. The first steps in this directions have been undertaken by Eden and Greatbatch (2008), Jayne (2009), and Nikurashin and Ferrari (2011), who parameterized the contribution from the conversion of the barotropic to the baroclinic tides, baroclinic instability, and lee waves, respectively. The present authors chose near-inertial waves (NIWs) as the next step for two reasons. First, it is a local problem, which makes it more tractable. Second, in contrast to most other sources of internal wave energy, which rely on conversion processes at the ocean bottom (i.e., tides, lee waves), the source region for locally wind-forced NIWs (the ocean mixed layer) is close to the thermocline. This makes directly forced NIWs more likely than other internal wave processes to affect air–sea fluxes and climate (cf. Jochum 2009; Jayne 2009).

The next section describes the model used, the Community Climate System Model, version 4 (CCSM4). Section 3 quantifies the strength of the NI currents in this model, describes how they can be amplified to match observed values, and how their effect on diapycnal mixing can be parameterized. Section 4 quantifies the impact of NIWs, first on the ocean mean state and then on climate by looking at the GCM solutions with and without NIWs. The last section provides a summary and discusses implications as well as shortcomings of the present study.

2. Model setup

The numerical experiments are performed using CCSM4, which consists of the fully coupled atmosphere, ocean, land, and sea ice models. A detailed description of this version can be found in Gent et al. (2011). The ocean component has a horizontal resolution that is constant at 1.125° in longitude and varies in latitude from 0.27° at the equator to approximately 0.7° in high latitudes. In the vertical there are 60 depth levels; the uppermost layer has a thickness of 10 m, the deepest layer has a thickness of 250 m. The atmospheric component uses a horizontal resolution of 0.9° × 1.25° (longitude and latitude, respectively) with 26 levels in the vertical. The sea ice model shares the same horizontal grid as the ocean model and the land model is on the same horizontal grid as the atmospheric model.

The vertical ocean surface boundary layer physics is represented by the *K*-profile parameterization (KPP) of Large et al. (1994). Diapycnal mixing beneath consists of the sum of four different processes: parameterized Kelvin–Helmholtz shear instability, parameterized double diffusion [for details on both see Large et al. (1994)], mixing associated with the conversion of the barotropic tide into baroclinic waves at topographic ridges (Jayne 2009), and a background internal wave diffusivity that varies in latitude (Jochum 2009) and is enhanced in the Banda Sea (Jochum and Potemra 2008). The spatial structure of this background diffusivity is a crude representation of processes as varied as reduced wave–wave interaction along the equator, parametric subharmonic instability of the M2 tide, and trapping of tidal energy in the Indonesian Seas.

This setup constitutes the released version of CCSM4, and further details can be found in Danabasoglu et al. (2012a). The control simulation for the present study is identical to the released version except for two changes: reduced background mixing in the Arctic Ocean (from 0.17×10^{-4} to 0.01×10^{-4} m^2 s^{-1} north of 70°N; Levine et al. 1985; Rudels et al. 1996), and increased mixing in the Banda Sea (from 1×10^{-4} to 3×10^{-4} m^2 s^{-1}; Gordon et al. 2010). These new values lead to only minor changes, mostly in Arctic sea surface salinity and tropical precipitation (not shown), but since they represent the current observational knowledge, they will be part of future model versions. This model version is initialized with year 863 from the output of the released version of CCSM4, then integrated for 100 years, and the mean of the last 40 years of this simulation will be referred to as CONT. The next section will describe how the control version of CCSM4 is modified to account for NIWs.

3. Representing oceanic near-inertial waves in a climate model

NIWs are ubiquitous to the ocean, but their generation, propagation, and demise are not well understood (e.g., Garrett 2001). It is clear, however, that much of the observed energy in the NIW band results from the accumulation of internal wave energy at their respective

turning latitudes (Fu 1981). Here we regard this energy as contributing to the background mixing, which is not part of the present study. Instead, we will focus only on the better accounting for the local generation of NIWs by wind, and their local dissipation to heat and potential energy in and below the boundary layer.

Much of what is known about NIWs builds on the observations and model studies of the Ocean Storms Experiment [D'Asaro 1995; see also Dohan and Davis (2011) for a summary of the outcomes and additional data]. Inertial oscillations of the boundary layer are a free mode of the ocean and they are its first response to changes in the wind stress (e.g., D'Asaro 1985). Most of the NIW energy is converted from kinetic energy to heat and potential energy through shear instability in the boundary layer (Large and Crawford 1995, hereafter LC95), with the remainder being either radiated away downward and equatorward (Alford and Zhao 2007), or converted locally beneath the boundary layer. Thus, for a realistic parameterization of the local NIW dissipation one has to ensure the right magnitude of NI energy input into the ocean model, and develop a representation of the NIW-induced mixing beneath the boundary layer.

To resolve the flux of NI energy E^i into the ocean, we changed the frequency at which wind stress is computed and passed to the ocean from the default of 1–12 times per day. This setup is initialized like CONT, also integrated for 100 yr, and the mean of the last 40 yr will be referred to as TWOH. To determine the simulated flux of NI energy into the ocean, wind stress and ocean surface velocity of year 21 are sampled every 2 h. The NI component of the velocity is determined with a zero-phase response Butterworth filter that retains the energy in the band between $0.7f$ and $1.3f$ (f being the local inertial frequency). This range brackets the spectral range where the energy is above the background values. The flux of E^i is then computed at every grid point as

$$E^i = u^i \tau_x + v^i \tau_y,$$

with u^i and v^i being the two horizontal near-inertial velocity components, and τ_x and τ_y the two wind stress components. The pattern of the resulting mean fluxes are similar to the results of Alford (2003), Jiang et al. (2005), and Furuichi et al. (2008), but the magnitude in TWOH is only 0.2 TW compared to the 0.3–1.4-TW estimates of the previous studies.

The spread in the estimates reflects the sensitivity of the NI energy fluxes to boundary layer physics (Plueddeman and Farrar 2006) and atmospheric resolution (Jiang et al. 2005). The Ocean Storms Experiment suggests that much of E^i is put into the ocean by the rapid rotation of the wind stress vector in an inertial sense across the semigeostrophic fronts of midlatitude storm systems (LC95). These fronts are not well resolved in the 200-km resolution National Centers for Environmental Prediction (NCEP) winds used by Alford (2003) and Hoskins (1983), nor are they resolved in the present 100-km-resolution version of CCSM4 (R. Neale 2012, personal communication). Thus, the present estimate of E^i represents a lower bound of the true air–sea flux of NIW energy. Additional constraints on this energy can be obtained from observations of surfaced Argo floats (Park et al. 2005) and surface drifters (Chaigneau et al. 2008; Elipot and Lumpkin 2008). These data suggest a global mean inertial current strength of approximately 10 cm s^{-1}. The strength of the NI currents in TWOH is shown in Fig. 1a, and it can be compared directly with Fig. 1b of Chaigneau et al. (2008). The pattern of NI current strength is similar between TWOH and the observations, with maxima under the midlatitude storm tracks and the deep tropics. The amplitude in TWOH, however, is only approximately half of the observed: the average between 50°S and 50°N is only 5 cm s^{-1} in TWOH compared to 10 cm s^{-1} from Chaigneau et al. (2008). Elipot and Lumpkin (2008) binned the data in zonally averaged bands and provide the latitudinal distribution of NI flow in the ocean. They find three maxima of E^i: in the northern and southern midlatitudes and the deep tropics. They are about equally strong with NI velocities between 14 and 18 cm s^{-1}, the former two are associated with the midlatitude storm tracks, and the latter results from the merger of the inertial frequency band with the energetic low-frequency band. These three maxima are also present in TWOH, with an amplitude of 6–7 cm s^{-1} in the midlatitudes, and an average of 12 cm s^{-1} for the domain between 10°S and 10°N. This suggests that in the deep tropics, where much of E^i comes from the energetic low-frequency band that is resolved in CCSM4 (Jochum et al. 2008), E^i levels are realistic; it is in the midlatitudes where they are too weak.

The challenge now is how to account for the lacking NIW activity. Most parameterizations represent a subgrid process that is missing altogether, so the effect of the process on the large-scale circulation has to be estimated from the properties of the large-scale circulation alone; eddy transport, for example, can be represented as diffusion working on the large-scale tracer gradients (Prandtl 1925). Here we are in the more fortunate position that the model produces NIWs; however, without sufficient resolution in the atmospheric model they are too weak and need to be amplified.

To do this, the inertial component of the simulated velocity has to be determined. At every time step the

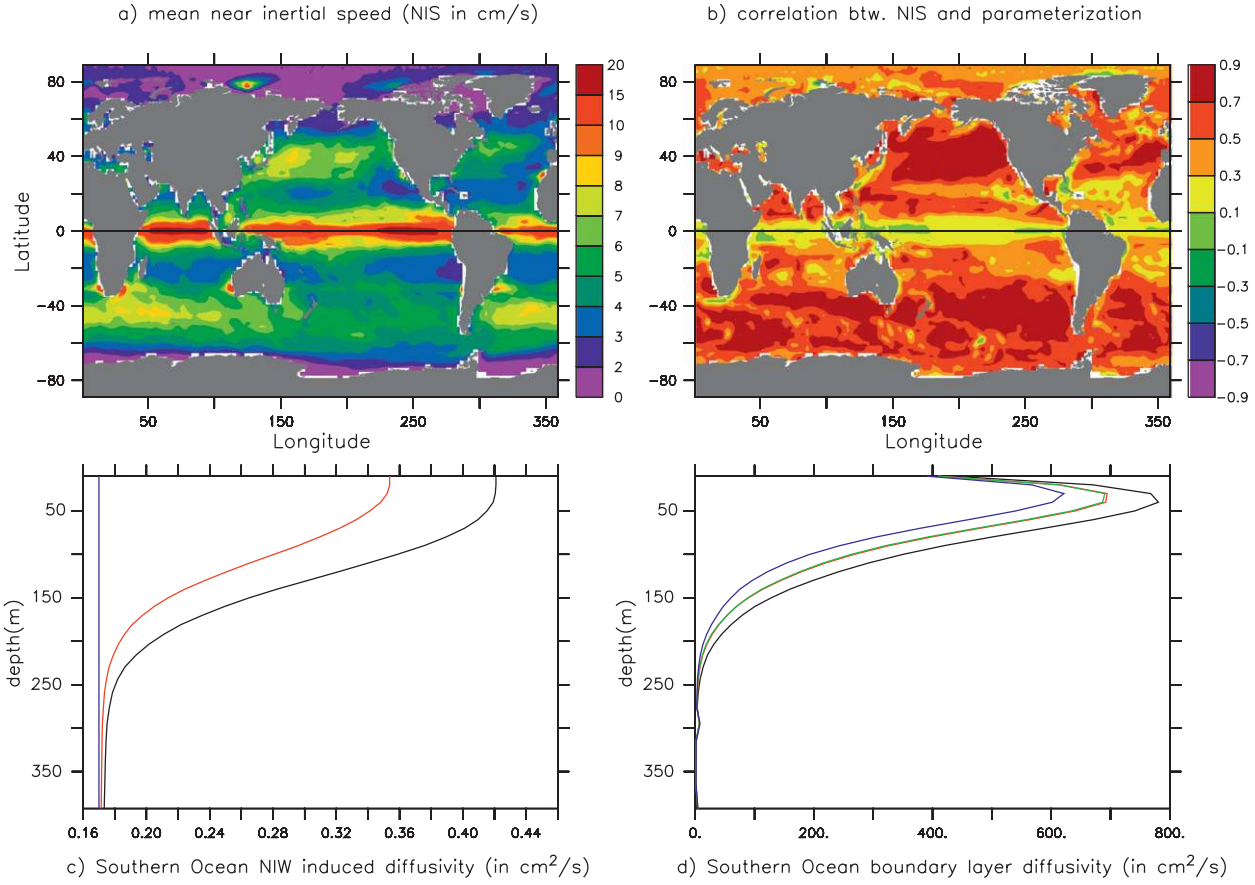

FIG. 1. (a) Global distribution of inertial current speed (in cm s^{-1}). (b) Correlation between the zonal component of inertial velocity (as determined with a bandpass filter) and its approximation (see text). (c) Diapycnal background diffusivities averaged across the Southern Ocean from 70° to 40°S in CONT (blue), TWOH+ (red), and FULL (black). Note that the abyssal component of Jayne (2009) and the boundary layer component of Large et al. (1994) are not included here. (d) Diapycnal boundary layer diffusivities averaged across the Southern Ocean from 70° to 40°S for CONT (blue), TWOH (green), TWOH+ (red), and FULL (black).

vector of the horizontal model velocity $\mathbf{u}$ contains the background flow and the signal from the resolved NIWs:

$$\mathbf{u} = \mathbf{u}^b + \mathbf{u}^i. \tag{1}$$

With 2-h coupling model time step is 48 min, and since outside the deep tropics the velocity changes on these time scales are dominated by NIWs (Crawford and Large 1996, hereafter CL96), we can write for the velocity at time t:

$$\mathbf{u}(t+1) - \mathbf{u}(t) \approx \mathbf{u}^i(t+1) - \mathbf{u}^i(t). \tag{2}$$

The velocity of inertial waves with period T can be described with

$$u^i = A\sin(2\pi/Tt) \quad ; \quad v^i = A\cos(2\pi/Tt), \tag{3}$$

(for the Northern Hemisphere, different signs apply for the Southern Hemisphere; LeBlond and Mysak 1978) from which follows:

$$u^i = -T/2\pi dv^i/dt. \tag{4}$$

Here dv^i/dt can, of course, be determined from two consecutive model time steps, so that

$$u^i(t+1) \approx -T/2\pi[v(t+1) - v(t)]/dt, \tag{5}$$

$$v^i(t+1) \approx T/2\pi[u(t+1) - u(t)]/dt. \tag{6}$$

Thus, outside the deep tropics the inertial part of the velocity can be recovered from the total velocity of two consecutive time steps (Fig. 1b).

NIWs mostly impact the large-scale circulation by increasing the shear in the upper ocean, which can lead to shear instability and a deepening of the boundary

layer (LC95; Dohan and Davis 2011). In CCSM4 this is represented within KPP, where boundary layer depth is defined as the depth where the bulk Richardson number equals the critical value of 0.3 ($\mathrm{Ri}_b = 0.3$):

$$h_b = \mathrm{Ri}_b[(u_1 - u_h)^2 + (v_1 - v_h)^2 + \gamma]/(b_1 - b_h), \quad (7)$$

where b_1 and b_h are the buoyancy at the surface and at the boundary layer depth, respectively; h_b is the boundary layer depth; and γ accounts for unresolved shear (Large et al. 1994). We note that in the original development and testing of the boundary layer model the structure of the atmospheric fronts is well resolved, so that the shear due to NIWs is not considered part of the unresolved shear (LC95; CL96). As shown here, this is not true anymore once the boundary layer model is part of a low-resolution coupled GCM. To account for the too weak NIWs in CCSM4 we therefore add a correction to the velocity shear in the KPP computation of the boundary layer depth:

$$h_b = \mathrm{Ri}_b[(u_1 + u_1^{\mathrm{unr}} - u_h - u_h^{\mathrm{unr}})^2 + (v_1 + v_1^{\mathrm{unr}} - v_h - v_h^{\mathrm{unr}})^2 + \gamma]/(b_1 - b_h), \quad (8)$$

with the unresolved part of the NIW velocities labeled $\mathbf{u}_h^{\mathrm{unr}}$. We estimated that the observed NI currents are approximately twice as strong as the simulated ones; thus, for a conservative implementation of the ideas above we increase their simulated strength by 80%:

$$\mathbf{u}_1^{\mathrm{unr}} = c\mathbf{u}_1^i, \quad (9)$$

with $c = 0.8$.

Regarding the correction at the boundary layer depth, we know that NIWs lose approximately 70%–90% of their energy in the boundary layer (LC96; Furuichi et al. 2008). They also lose their coherence (Dohan and Davis 2011), so that in the absence of more observations and better theoretical understanding $\mathbf{u}_h^{\mathrm{urn}}$ is assumed to be negligible: $\mathbf{u}_h^{\mathrm{unr}} = 0$. These corrections are applied fully only poleward of 10° latitude and taper off to 0 at 5° latitude; equatorward of this latitude the velocity changes from time step to time step are not dominated anymore by NIWs (Fig. 1b), and fortunately, as discussed above, the biases of the modeled inertial velocities in the deep tropics are minor. We expect that the appropriate value of c is model dependent; in particular it should be a function of the spatial and temporal resolution of the atmospheric forcing. If the ocean and atmospheric component of the GCM both resolve the atmospheric fronts in the mid- and high-latitude storm systems this factor should be 0.

While the boundary layer part of the NIWs only needs amplification, the part that escapes needs to be parameterized, because the ocean model resolution is not sufficient to represent the propagation of NIWs away from the boundary layer. The mixing beneath the boundary layer is based on a fraction of inertial energy that enters the boundary layer, and is distributed vertically assuming an exponential decay in an approach similar to the one of Jayne and St. Laurent (2001; Jayne 2009). This fraction and its exponential decay scale can be estimated from observations and numerical simulations. Alford and Whitmont (2007) observe a vertical decay scale of 2000 m, CL96 estimate that 70%–80% of the NI energy is dissipated in the boundary layer (boundary layer fraction bf = 0.7), and Furuichi et al. (2008) find that approximately half of the NI energy that makes it beneath the boundary layers of the North Pacific and the Southern Ocean radiates away (local fraction lf = 0.5). The latter two are numerical studies, but CL96 has been validated with the Ocean Storms data, and the Furuichi et al. (2008) results compare well with the flux estimates of Alford and Zhao (2007). Thus, below the boundary layer the energy flux available for mixing from locally generated NIWs is

$$\epsilon = \epsilon^i \times (1 - \mathrm{bf}) \times \mathrm{lf}, \quad (10)$$

where ϵ^i is the energy flux in the inertial band that enters the boundary layer. The diapycnal mixing that is caused by the downward-propagating NIWs can then be computed with the Osborn (1980) relation between diffusivity and dissipation:

$$k_{\mathrm{niw}} = \frac{\Gamma \epsilon F(z)}{\rho N^2}, \quad (11)$$

where $\Gamma = 1/(1 + 0.2) \approx 0.2$ is the mixing efficiency, N^2 is the local stratification, and $F(z)$ is a vertical structure function with a vertical scale of $\zeta = 2000$ m and a vertical integral value of 1 (St. Laurent and Nash 2004):

$$F(z) = \frac{e^{(z-h)/\zeta}}{\zeta(1 - e^{-h/\zeta})}, \quad (12)$$

which decays exponentially from the bottom of the boundary layer at depth h. The mixing efficiency determines what part of the available turbulent kinetic energy production ϵ is available for mechanical work. The value of 0.2 is based on laboratory work as well as theoretical considerations (e.g., Ivey and Imberger 1991) and it means that 20% of ϵ are used to increase the potential energy of the fluid, and 80% is dissipated to heat the fluid (not considered here).

What remains is the determination of ϵ^i, the inertial energy entering the boundary layer at every model time step. As with inertial velocities poleward of 10° latitude, the inertial energy flux into the boundary layer can be computed from the difference in kinetic energy between two consecutive time steps. However, k_{niw} must be positive definite, whereas the change of kinetic energy in the boundary layer can be positive as well as negative. Of course, the time integral of NI energy flux is always positive for time scales longer than a month; however, the model has only two time steps available, which in the present case are only 48 min apart. Since we cannot simulate individual NIW groups, but want to capture the seasonality of the mixing due to varying storm intensity, we decided on a formulation that uses only the absolute value of the boundary layer kinetic energy change:

$$\epsilon^i(t+1) = \alpha|\mathrm{blke}(t+1) - \mathrm{blke}(t)|/dt, \qquad (13)$$

where blke is the kinetic energy of the boundary layer, and α is a scaling factor that ensures that the global, annual mean value of ϵ^i matches the 0.2 TW determined from TWOH (here: $\alpha = 0.05$). This scaling factor is determined empirically here, but it is consistent with the values obtained by CL96 for large ensembles of simulated midlatitude storms (see their Fig. 15).

This subboundary parameterization for NIW-induced mixing is added to TWOH, and a third fully coupled 100-yr integration is performed (TWOH+). Admittedly this parameterization is rather crude, but it turns out that the biggest impact of NIWs comes from their increasing the shear in the boundary layer, and not from the increased diapycnal mixing beneath. This is simply because the energy levels are rather low: $\Gamma \times (1 - \mathrm{bf}) \times \mathrm{lf} \times 0.2\,\mathrm{TW} = 0.006\,\mathrm{TW}$, which is 2% of the energy used by the models mixing beneath the boundary layer. The resulting diffusivities rise above the background only near the surface (Fig. 1c). Note that these diffusivities are consistent with the direct observations by Ledwell et al. (2011), who in the southeast Pacific find values in excess of 0.2 $\mathrm{cm^2\ s^{-1}}$ only in the upper 200 m. The 0.3 TW of total energy that is used for the mixing below the boundary layer is also consistent with the 0.4 TW estimated from observations (Wunsch and Ferrari 2004). Note that the experiment TWOH+ did not feature the reduction of diffusivity in the Arctic. This is an oversight, so that the comparison between TWOH and TWOH+ is not quite clean. However, the comparisons above are done in the Southern Ocean, and because of the earlier result that reduced Arctic diffusivity has only little global impact (see section 2), the authors felt the expense of another long coupled integration was unwarranted.

TABLE 1. List of experiments.

Expt	Coupling period	α	c
CONT	24 h	0	0
TWOH	2 h	0	0
TWOH+	2 h	0.05	0
FULL	2 h	0.1	0.8

In summary, apart from CONT three model setups are integrated that are identical to CONT except for the changes discussed above: TWOH, where the coupling interval is changed from 24 to 2 h; TWOH+, where the coupling interval is 2 h and the NIW-induced mixing below the boundary layer is parameterized; and FULL, which has a coupling interval of 2 h, and where the lack of NIW energy in TWOH+ is compensated by increasing the shear in the boundary layer as described above, and by doubling the amount of energy available for mixing beneath the boundary layer (see Table 1). The focus of the next section will be a comparison between FULL and CONT, which leads to an estimate of the impact that NIWs have on climate. The other two integrations are not discussed here in detail; for the most part the differences between TWOH and CONT are about half of the differences between FULL and CONT, with TWOH+ being similar to TWOH. This is illustrated for diapycnal diffusivity in Fig. 1d.

4. Results

Accounting for NIWs in CCSM4 leads to a deepening of the boundary layer, mostly in the regions dominated by trades and westerlies (Fig. 2). Determining and comparing boundary layer depths, which is a model diagnostic, with observed mixed layer depths, whose determination is ambiguous, is fraught with difficulties. Danabasoglu et al. (2012a), however, showed that the mixed layer depths in CCSM4 are generally too shallow, so that accounting for NIWs leads to a widespread improvement. An artificial passive tracer called Ideal Age is used to establish whether the improved boundary layer depth leads to better ventilation of the intermediate waters, a possibly related bias in CCSM4 (Danabasoglu et al. 2012a). The value of this tracer is set to zero in the surface layer, and increased by *dt* for every model time step it spends below the surface. Below 300-m depth, however, the Ideal Ages in CONT and FULL are not significantly different (not shown). Thus, contrary to our expectations, NIWs do not contribute to the ventilation of the deep ocean, nor do they lead to a significant change in the Atlantic meridional overturning circulation (AMOC) or northward heat transport (not shown). As shown below, however, their impact on the sea surface temperature

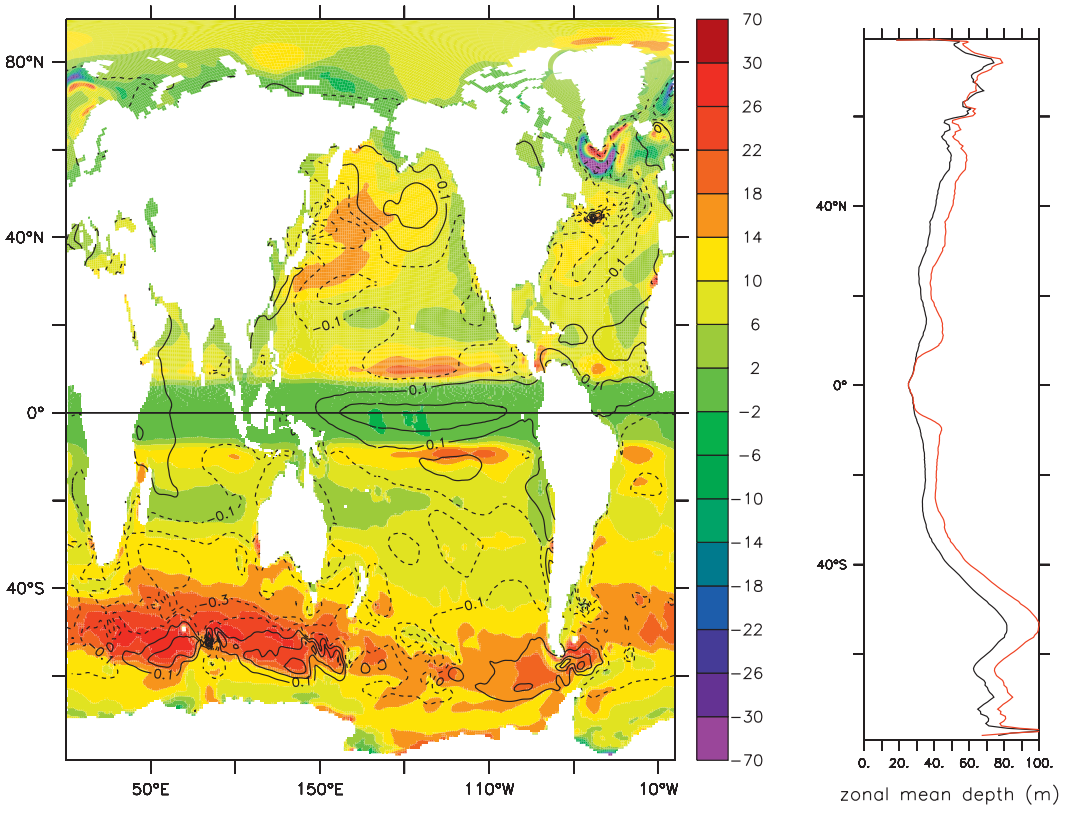

FIG. 2. (left) Difference in annual mean boundary layer depth between FULL and CONT (color, in m), and their difference in SST (contour interval is 0.2°C, maximum cooling is 1.5°C in the Kuroshio). Note that the large differences off Svalbard and Greenland are not significant; they are connected to a multidecadal oscillation in the AMOC (Danabasoglu et al. 2012b). (right) Zonally averaged boundary layer depth in CONT (black) and FULL (red).

(SST) affects tropical precipitation and the large-scale atmospheric circulation.

NIWs cool the SST throughout the subtropics (Fig. 2) by mixing heat downward, which increases the average net ocean heat uptake by 0.24 W m^{-2} from a global cooling of 0.12 to a global warming of 0.12 W m^{-2}. Locally, the largest changes to the net surface heat flux are related to changes in the sea ice concentration. In particular in the Southern Ocean the weaker westerlies in FULL (see below) lead to a weaker equatorward Ekman drift, which reduces the sea ice extent but increases the sea ice concentration along the coasts (Fig. 3). Correspondingly the heat loss in FULL is reduced along the Antarctic coast and increased farther offshore along the position of the sea ice edge in CONT (Fig. 3). These differences compensate, so that the area south of 57°S has the same net heat loss in FULL and CONT. Between 57° and 30°S the NIW induced cooling of the SST leads to an increased heat uptake of 1.0 W m^{-2}, all of which is then lost again to the atmosphere between 30°S and 8°N. Finally, the latitude band between 8° and 20°N increases its net heat uptake in FULL by 2.2 W m^{-2}, and the ocean farther north has no net change in the heat uptake.

What emerges from these numbers and from Fig. 3 is that in the subtropics heat is removed from the surface and pumped beneath the boundary layer. A small fraction of it is pumped beneath the thermocline where it contributes to the overall warming trend of the ocean. Most of the heat, though, results in warmer thermocline water (see Fig. 3) that is advected to the equatorial upwelling regions (Pedlosky 1987; McCreary and Lu 1994) and leads to a warming of the equatorial SST (Fig. 2). The resulting changes in tropical SST are small, but prior studies with coupled models have already shown that even small changes can lead to large-scale rearrangements of the Hadley and Walker circulations (e.g., Jochum and Potemra 2008). This is because tropical atmospheric circulation depends on the absolute SST as much as on its gradient (Lindzen and Nigam 1987) and the location of its maximum (Gill 1980).

The position of the maximum annual mean SST in both simulations is the same (southern part of the western Pacific warm pool), but the SST gradients have

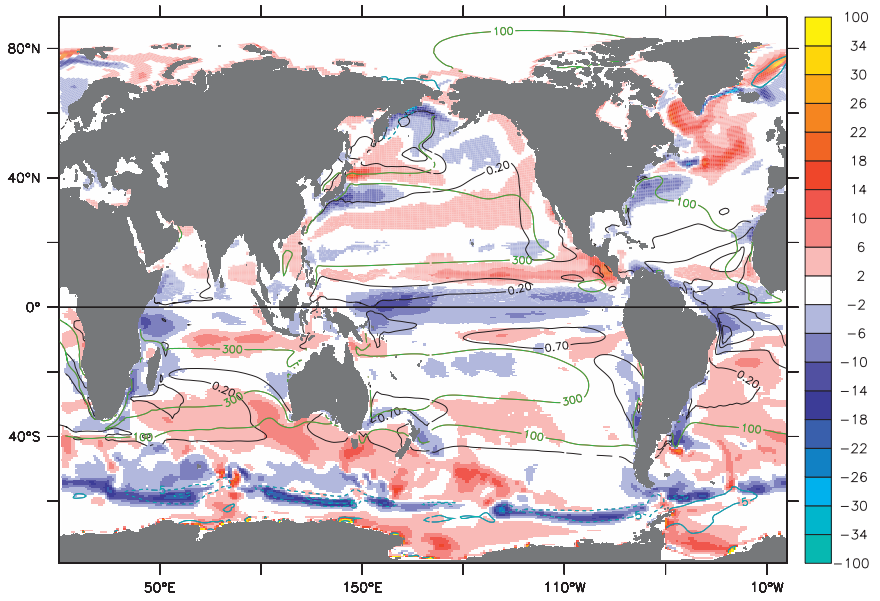

FIG. 3. Difference in net surface heat flux (color, in W m^{-2}) and temperature on the 26σ isopycnal of CONT (contour interval 0.5°C, starting at 0.2°C). The largest warming on this isopycnal occurs off Brazil with a 1.8°C warming. For orientation, the depth of the 26σ isopycnal in CONT is indicated through the 100- and 300-m isobaths in green. The differences in sea ice concentration are shown in blue (contour interval is 10%). All differences are FULL-CONT.

changed. For example, a zonal average over the Atlantic basin SST shows that difference between the SST maximum north of the equator and the minimum on the equator has been increased from 0.8° to 0.9°C. In the Pacific, this difference has been reduced from 1.4° to 1.2°C. These differences fall within the observational uncertainty of SST (e.g., Hurrell and Trenberth 1999), but they are large enough to force a shift in precipitation from the cooled to the heated regions (Fig. 4a). Interestingly, the shift has a pattern similar to the long-standing precipitation biases of CCSM4 (Fig. 4c): in all three basins there is too much rain south of the equator, in the Atlantic there is too little to the north of the equator, and the Pacific intertropical convergence zone (ITCZ) is too far north of the equator.

The shifts in deep convection associated with the SST changes generate planetary waves that change global patterns of sea level pressure (e.g., Sardeshmukh and Hoskins 1988). In general the sea level pressure is increased over the poles and reduced over the midlatitudes (Fig. 4a). It is difficult, if not impossible, to associate unambiguously particular sea level pressure changes with particular convection changes (Ting and Sardeshmukh 1993). The present differences between FULL and CONT, however, are quite similar to the pressure differences induced by the El Niño of 1986/87 (Trenberth et al. 1998): a weakening of the pressure difference between the Azores and Iceland, and a weakening of the pressure gradient across the Southern Ocean (Fig. 4a). This suggests that the ultimate source of the difference in global sea level pressure is the warming of the eastern equatorial Pacific. In turn, the change in sea level pressure leads to reduced wind stress, in particular the westerlies over the North Atlantic and the Indo-Pacific sector of the Southern Ocean have been weakened (Fig. 4b).

A comparison of Fig. 4a with Fig. 4c shows that the pattern of precipitation and sea level pressure differences are similar to the one of the CCSM4 biases. The changes to sea level pressure lead to a reduced meridional pressure gradient and explain the weaker westerlies seen in Fig. 4b. The weaker westerlies lead to a reduced equatorward Ekman drift of sea ice (Holland and Raphael 2006), which in the present case leads to a reduction in sea ice concentrations along the Southern Ocean and North Atlantic sea ice edge of up to 20% (Fig. 3). In the Southern Ocean The weaker westerlies also reduce the equatorward Ekman transport (the maximum of the zonally averaged northward flow is reduced by 15%) of cold polar water, which explains why there the SST is warmer despite the increased vertical mixing and increased heat loss (Figs. 2 and 3). On the other hand, the increased SST in the northern North Pacific is not associated with a weakening of the westerlies. Unlike most of the rest of the ocean, this area is characterized by a surface layer of relatively cold and freshwater, overlaying

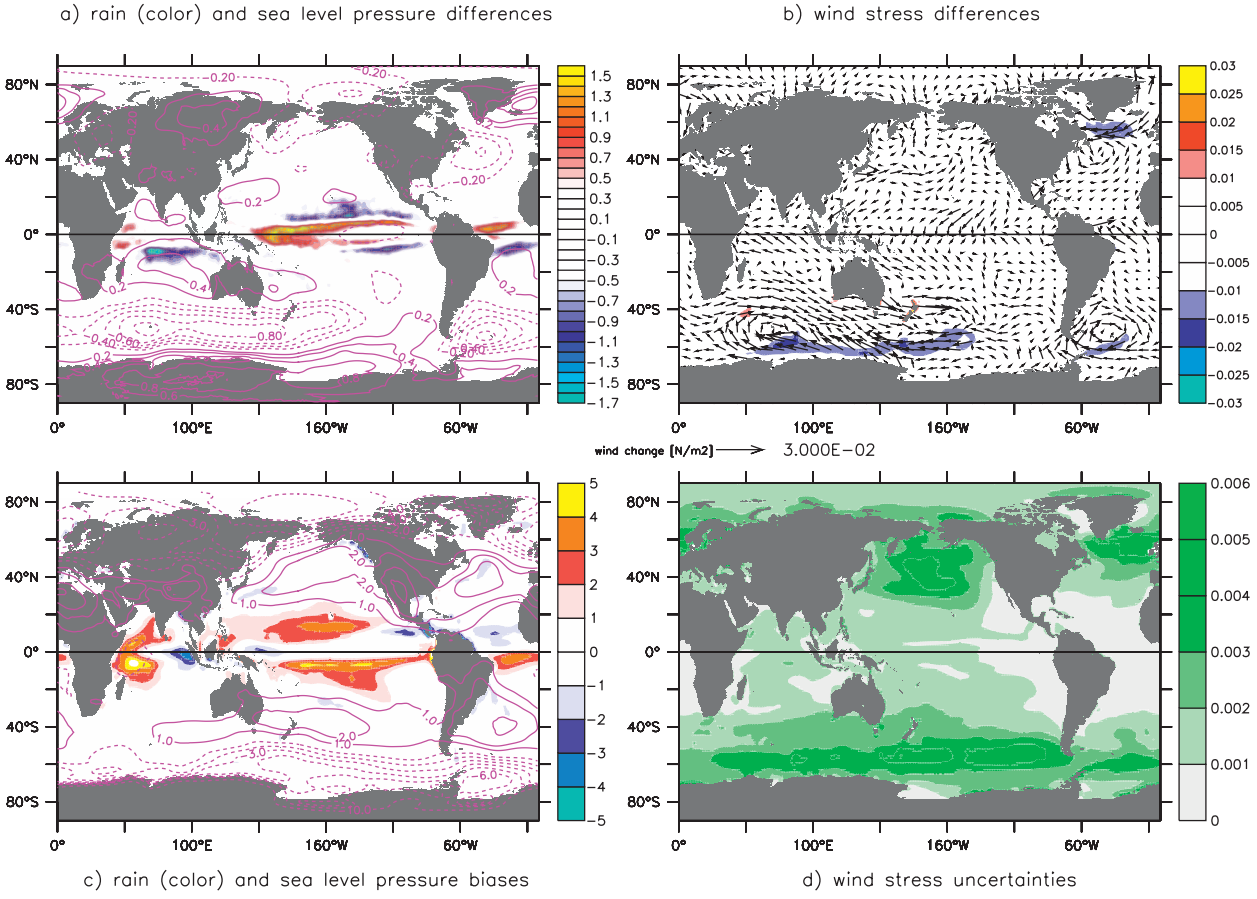

FIG. 4. (a) Difference in annual mean precipitation between FULL and CONT (color, in mm day^{-1}), and the difference in sea level pressure (contour interval 0.2 mb; the largest differences are the 1.2-mb increase off Iceland, and the 1.6-mb increase off Marie Byrd Land). (b) Difference between FULL and CONT in annual mean winds stress (vectors) and annual mean zonal wind stress (color, in N m^{-2}). (c) Differences between CONT and observations (Large and Yeager 2008) in sea level pressure (contour interval 1 mb) and precipitation (color, in mm day^{-1}). (d) Uncertainty of the annual means of zonal wind stress in CONT, based on 40 years (in N m^{-2}).

warmer and saltier water (Tsuchiya 1982). The larger mixing in FULL pushes the boundary layer into this temperature inversion (at depths between 30 and 100 m), and leads to a warmer SST than in CONT.

The general deepening of the boundary layer in response to NIW-induced mixing that is described here is not surprising. The tropical precipitation feedback is unexpected but consistent with several previous studies that are mentioned above. However, the strong response of the westerlies, and the similarity to the pattern of model biases, requires more statistics than mere trust in a 40-yr average. Figure 4d shows the uncertainty of the annual mean zonal wind stress assuming every year is independent from the next one (computed as the standard deviation of the annual mean divided by the square root of 40). In the North Atlantic and the Southern Ocean areas of large differences between FULL and CONT these uncertainties are approximately only one-fifth of the signal. Of course, these are also areas with interannual- to decadal-scale variability (North Atlantic Oscillation and southern annular mode), but a Student's *t* test for the years 21–100 of CONT and FULL reveals that the colored areas in Fig. 4b are significantly different from each other at the 95% level.

5. Summary and discussion

The present study is a first attempt to quantify the impact of wind-generated NIWs on climate. Even with 2-hourly coupling the mixed layer speeds of the NIWs are too weak outside the deep tropics, and the part of the NIWs that radiates away beneath the mixed layer is not represented at all. Thus, the mixed layer part of the NIWs has to be amplified and the effect of the radiating part on diffusivity has to be parameterized. Here is the full list of ideas and assumptions that is needed to estimate the effect of NIWs on climate in CCSM4:

- 2-hourly coupling instead of daily coupling.
- Outside the deep tropics the resulting NIWs need to be amplified in the mixed layer by 80%.
- The main effect of NIWs in the mixed layer is captured by representing their shear in the Richardson number computation of the mixed layer scheme.
- The coherent part of the NIW velocities at the bottom of the mixed layer is negligible.
- On the time scale of a model time step (around 1 h), velocity fluctuations outside the deep tropics are dominated by NIWs.
- Of the total NIW energy flux that enters the ocean, 30% is available for mixing beneath the mixed layer.
- Similar to the NIW velocites, this energy flux can be estimated from mixed layer kinetic energy fluctuations.
- 50% of this sub–mixed layer energy is available for local mixing with a vertical decay scale of 2000 m.
- The other 50% radiate away and are not considered here.

Each of these statements has been motivated by observations, if possible, and numerical model results, but they are associated with large uncertainties.

Using the ideas and assumption listed above, the effect of NIW mixing is quantified by making three changes to the standard configuration of CCSM4. First, the period of coupling between the atmosphere and the ocean model is reduced from 1 day to 2 h. Second, outside the deep tropics the near-inertial component of the ocean surface velocity is determined by using the ocean model as a bandpass filter, and the shear that is used to compute the boundary layer depth is increased to account for the too weak NI velocities in CCSM4. Last, the air–sea flux of NIW energy into the boundary layer is determined, and 15% of it is used to increase the background diffusivity below the boundary layer. All three changes increase mixing and deepen the mixed layers. They do not improve the ventilation of the subthermocline because most of the NIW energy is used up in the mixed layer and only a little is left for mixing beneath the mixed layer. While the deepening of the mixed layer does not lead to a better ventilation below the thermocline, it does lead to a change in SST: cooling in the subtropics and deep tropics as direct response to the increased mixing, warming in the tropical and equatorial upwelling that are fed by these warmer waters, and warming under the midlatitude westerlies as a result of atmospheric teleconnections. In the tropics, these SST changes are generally less than 0.5°C, but this is sufficient to cause a shift in tropical precipiation and via atmospheric teleconnections a reduction in midlatitude wind stress. This tropical sensitivity is consistent with earlier tropical mixing studies (e.g., Jochum and Potemra 2008), and it is because of this sensitivity that more research is required. In particular there are two major factors that contribute to the uncertainty in the present results.

First, the main uncertainty lies with the estimates of the true E^i. Estimating this flux requires collocated ocean velocity and wind data, which are only available from a few moorings (e.g., Alford et al. 2012). Thus, global estimates are by necessity based on a combination of atmospheric reanalysis products (obtained with a numerical model; e.g., Kalnay et al. 1996), and a mixed layer model with reduced physics (with its own problems; e.g., Plueddeman and Farrar 2006). The global flux estimates by Jiang et al. (2005) range from 0.3 to 1.4 TW, so that the present results, which are based on a value of 0.36 TW, are probably a conservative estimate of the NIW impact. To overcome the fundamental uncertainty that is created by combining reanalysis products with simple mixed layer models, one needs to use a GCM that fully resolves tropical and extratropical cyclones (e.g., McClean et al. 2011). This is still only a model, but this framework is using sophisticated air–sea coupling techniques, as well as resolving the frontal systems of storms (J. Tribbia 2012, personal communication).

Second, apart from the magnitude of the wind energy source, there are considerable uncertainties in the pattern of the implemented NIW mixing. The present mixed layer parameterization has been developed with midlatitude storm systems in mind (LC95) and has also been tested extensively with observations from the equatorial Pacific (e.g., Large and Gent 1999; Wang et al. 1996). Furthermore, comparing Fig. 1a with observations suggests that near the equator the model's representation of the NI velocity is adequate, and Fig. 1b demonstrates that the present amplification of NI velocities in mid- to high latitudes is reasonable. What is unclear is what should be done in the area between 5° and 15° of latitude. In this area the model may underestimate the NI velocities, but the correlation between the bandpass-filtered NI velocities and its parameterization starts to break down. The present solution is to gradually reduce the magnitude of the parameterized NI velocity component [Eq. (9)] from a factor of 1 at 10° latitude to a factor of 0 at 5° latitude. This is defendable in the absence of more detailed observations, but unfortunately this is also the area where the atmosphere is most sensitive to SST changes. Thus, a second focus of future NIW research should be an analysis of the available tropical mooring records to obtain a detailed picture of the subtropical to equatorial change of the NIW fields.

Last, the impact of directly generated NIWs on diapycnal mixing below the boundary layer requires more scrutiny. In section 3 it is estimated that NIWs contribute

no less than 2% of the energy for the background mixing. This appears negligible, but it has to be remembered that the uncertainties are large. As emphasized above, the air–sea flux of NI energy could be a factor of 6 larger than assumed in section 3 (Jiang et al. 2005), and this alone would bring the contribution up to 12%. The recent analysis of the Ocean Station Papa data suggests that up to 50% of the NIW energy could escape the boundary layer (rather than the 30% assumed here; Alford et al. 2012). Furthermore, the present study only considers the local effects of NIW generation; the other half of the energy that escapes the boundary layer has eventually to be accounted for. In light of their spatial inhomogeneity, it is therefore conceivable that in some regions NIWs could contribute a third of the energy for the background mixing. Key again here is the total amount of NI energy generated directly by the wind, which in the present study appears to be largest source of uncertainty.

Acknowledgments. This research was funded as part of the Climate Process Team on internal wave-driven mixing with NSF Grant Nr E0968771 at NCAR. The computational resources were provided by the Computational Information Systems Laboratory at NCAR.

REFERENCES

Alford, M. H., 2003: Improved global maps and 54-year history of wind-work on ocean inertial motions. *Geophys. Res. Lett.,* **30,** 1424, doi:10.1029/2002GL016614.

——, and M. Whitmont, 2007: Seasonal and spatial variability of near-inertial kinetic energy from historical moored velocity records. *J. Phys. Oceanogr.,* **37,** 2022–2037.

——, and Z. Zhao, 2007: Global patterns of low-mode internal-wave propagation. Part I: Energy and energy flux. *J. Phys. Oceanogr.,* **37,** 1829–1848.

——, M. F. Cronin, and J. M. Klymak, 2012: Annual cycle and depth penetration of wind-generated near-inertial internal waves at Ocean Station Papa in the northeast Pacific. *J. Phys. Oceanogr.,* **42,** 889–909.

Chaigneau, A., O. Pizarro, and W. Rojas, 2008: Global climatology of near-inertial current characteristics from Lagrangian observations. *Geophys. Res. Lett.,* **35,** L13603, doi:10.1029/2008GL034060.

Crawford, G. B., and W. G. Large, 1996: Numerical investigation of resonant inertial response of the ocean to wind forcing. *J. Phys. Oceanogr.,* **26,** 873–891.

Danabasoglu, G., and J. Marshall, 2007: Effects of vertical variations of thickness diffusivity in an ocean general circulation model. *Ocean Modell.,* **18,** 122–141.

——, S. C. Bates, B. P. Briegleb, S. R. Jayne, M. Jochum, W. G. Large, S. Peacock, and S. G. Yeager, 2012a: The CCSM4 ocean component. *J. Climate,* **25,** 1361–1389.

——, S. G. Yeager, Y.-O. Kwon, J. J. Tribbia, A. S. Phillips, and J. W. Hurrell, 2012b: Variability of the Atlantic meridional overturning circulation in CCSM4. *J. Climate,* **25,** 5153–5172.

D'Asaro, E. A., 1985: The energy flux from the wind to near-inertial motions in the surface mixed layer. *J. Phys. Oceanogr.,* **15,** 1043–1059.

——, 1995: A collection of papers on the Oecan Storms Experiment—An introduction. *J. Phys. Oceanogr.,* **25,** 2817–2818.

Dohan, K., and R. E. Davis, 2011: Mixing in the transition layer during two storm events. *J. Phys. Oceanogr.,* **41,** 42–66.

Eden, C., and R. J. Greatbatch, 2008: Diapycnal mixing by mesoscale eddies. *Ocean Modell.,* **23,** 113–120.

Elipot, S., and R. Lumpkin, 2008: Spectral description of oceanic near-surface variability. *Geophys. Res. Lett.,* **35,** L05606, doi:10.1029/2007GL032874.

Fu, L.-L., 1981: Observations and models of inertial waves in the deep ocean. *Rev. Geophys. Space Phys.,* **19,** 141–170.

Furuichi, N., T. Hibiya, and Y. Niwa, 2008: Model-predicted distribution of wind-induced internal wave energy in the world's oceans. *J. Geophys. Res.,* **113,** C09034, doi:10.1029/2008JC004768.

Garrett, C., 2001: What is the ''near-inertial'' band and why is it different from the rest of the internal wave spectrum? *J. Phys. Oceanogr.,* **31,** 962–971.

Gent, P. R., and Coauthors, 2011: The Community Climate System Model version 4. *J. Climate,* **24,** 4973–4991.

Gill, A., 1980: Some simple solutions for heat-induced tropical circulation. *Quart. J. Roy. Meteor. Soc.,* **106,** 447–462.

Gordon, A. L., and Coauthors, 2010: The Indonesian Throughflow during 2004-2006 as observed by the INSTANT program. *Dyn. Atmos. Oceans,* **50,** 115–128.

Holland, M. M., and M. N. Raphael, 2006: Twentieth century simulation of the southern hemisphere climate in coupled models. Part II: Sea ice conditions and variability. *Climate Dyn.,* **26,** 229–245.

Hoskins, B., 1983: Dynamical processes in the atmosphere and the use of models. *Quart. J. Roy. Meteor. Soc.,* **109,** 1–21.

Hurrell, J. W., and K. E. Trenberth, 1999: Global SST analyses: Multiple problems and their implications for climate analysis. *Bull. Amer. Meteor. Soc.,* **80,** 2661–2678.

Ivey, G. N., and J. Imberger, 1991: On the nature of turbulence in a stratified fluid. Part I: The energetics of mixing. *J. Phys. Oceanogr.,* **21,** 650–658.

Jayne, S. R., 2009: The impact of abyssal mixing parameterizations in an ocean general circulation model. *J. Phys. Oceanogr.,* **39,** 1756–1775.

——, and L. C. St. Laurent, 2001: Parameterizing tidal dissipation over rough topography. *Geophys. Res. Lett.,* **28,** 811–814.

Jiang, J., Y. Liu, and W. Perrie, 2005: Estimating the energy flux from the wind to ocean inertial motions: The sensitivity to surface wind fields. *Geophys. Res. Lett.,* **32,** L15610, doi:10.1029/2005GL023289.

Jochum, M., 2009: Impact of latitudinal variations in vertical diffusivity on climate simulations. *J. Geophys. Res.,* **114,** C01010, doi:10.1029/2008JC005030.

——, and J. Potemra, 2008: Sensitivity of tropical rainfall to Banda Sea diffusivity in the Community Climate System Model. *J. Climate,* **21,** 6445–6454.

——, G. Danabasoglu, M. Holland, Y.-O. Kwon, and W. Large, 2008: Ocean viscosity and climate. *J. Geophys. Res.,* **113,** C06017, doi:10.1029/2007JC004515.

——, A. Jahn, S. Peacock, D. A. Bailey, J. T. Fasullo, J. Kay, S. Levis, and B. Otto-Bliesner, 2012: True to Milankovitch: Glacial inception in the new Community Climate System Model. *J. Climate,* **25,** 2226–2239.

Kalnay, E., and Coauthors, 1996: The NCEP/NCAR 40-Year Reanalysis Project. *Bull. Amer. Meteor. Soc.,* **77,** 437–471.

Large, W. G., and G. B. Crawford, 1995: Observations and simulations of upper-ocean response to wind events during the Ocean Storms Experiment. *J. Phys. Oceanogr.,* **25,** 2831–2852.

——, and P. Gent, 1999: Validation of vertical mixing in an equatorial ocean model using large eddy simulations and observations. *J. Phys. Oceanogr.,* **29,** 449–464.

——, and S. Yeager, 2008: The global climatology of an interannually varying air-sea flux dataset. *Climate Dyn.,* **33,** 341–364, doi:10.1007/s00382-008-00441-3.

——, J. C. McWilliams, and S. C. Doney, 1994: Oceanic vertical mixing—A review and a model with nonlocal parameterization. *Rev. Geophys.,* **32,** 363–403.

LeBlond, P. H., and L. A. Mysak, 1978: *Waves in the Ocean.* Elsevier, 616 pp.

Ledwell, J. R., L. C. St. Laurent, J. B. Girton, and J. M. Toole, 2011: Diapycnal mixing in the Antarctic Circumpolar Current. *J. Phys. Oceanogr.,* **41,** 241–246.

Levine, M., C. Paulson, and J. Morison, 1985: Internal waves in the Arctic Ocean—Comparison with lower latitude observations. *J. Phys. Oceanogr.,* **15,** 800–809.

Lindzen, R., and S. Nigam, 1987: On the role of SST gradients in forcing low level winds and convergence in the tropics. *J. Atmos. Sci.,* **44,** 2418–2436.

Liu, Z., and Coauthors, 2009: Transient simulation of last deglaciation with a new mechanism for Bolling–Allerod warming. *Science,* **325,** 310–314.

McClean, J. L., and Coauthors, 2011: A prototype two-decade fully-coupled fine-resolution CCSM simulation. *Ocean Modell.,* **39,** 10–30.

McCreary, J., and P. Lu, 1994: Interaction between the subtropical and equatorial ocean circulations: The subtropical cell. *J. Phys. Oceanogr.,* **24,** 466–497.

Munk, W., and C. Wunsch, 1998: Abyssal recipies II: Energetics of tidal and wind mixing. *Deep-Sea Res. I,* **45,** 1977–2010.

Nikurashin, M., and R. Ferrari, 2011: Global energy conversion rate from geostrophic flows into internal lee waves in the deep ocean. *Geophys. Res. Lett.,* **38,** L08610, doi:10.1029/2011GL046576.

Osborn, T. R., 1980: Estimates of the local rate of vertical diffusion from dissipation measurements. *J. Phys. Oceanogr.,* **10,** 83–89.

Park, J. J., K. Kim, and B. A. King, 2005: Global statistics of inertial motions. *Geophys. Res. Lett.,* **32,** L14612, doi:10.1029/2005GL023258.

Pedlosky, J., 1987: An inertial theory for the equatorial undercurrent. *J. Phys. Oceanogr.,* **17,** 1978–1985.

Plueddeman, A. J., and J. T. Farrar, 2006: Observations and models of the energy flux from the wind to mixed-layer inertial currents. *Deep-Sea Res. II,* **53,** 5–30.

Prandtl, L., 1925: Bericht über Untersuchungen zur ausgebildeten Turbulenz. *Z. Angew. Math. Mech.,* **5,** 136–139.

Rudels, B., L. Anderson, and E. Jones, 1996: Formation and evolution of the surface mixed layer and halocline of the Arctic Ocean. *J. Geophys. Res.,* **101** (C4), 8807–8822.

Sardeshmukh, P. D., and B. J. Hoskins, 1988: The generation of global rotational flow by steady idealized tropical divergence. *J. Atmos. Sci.,* **45,** 1228–1251.

St. Laurent, L. C., and J. D. Nash, 2004: An examination of the radiative and dissipative properties of deep ocean internal tides. *Deep-Sea Res. II,* **51,** 3029–3042.

Tandon, A., and C. Garrett, 1996: On a recent parameterization of mesoscale eddies. *J. Phys. Oceanogr.,* **26,** 406–411.

Ting, M. F., and P. D. Sardeshmukh, 1993: Factors determining the extratropical response to equatorial diabatic heating anomalies. *J. Atmos. Sci.,* **50,** 907–918.

Trenberth, K. E., G. W. Branstator, D. Karoly, A. Kumar, N.-C. Lau, and C. Ropelewski, 1998: Progress during TOGA in understanding and modeling global teleconnections associated with tropical sea surface temperatures. *J. Geophys. Res.,* **103** (C7), 14 291–14 324.

Tsuchiya, M., 1982: On the Pacific upper-water circulation. *J. Mar. Res.,* **40,** 777–799.

Wang, D. L., W. G. Large, and J. C. McWilliams, 1996: Large-eddy simulation of the equatorial ocean boundary layer: Diurnal cycling, eddy viscosity, and horizontal rotation. *J. Geophys. Res.,* **101** (C2), 3649–3662.

Wittenberg, A. T., 2009: Are historical records sufficient to constrain ENSO simulations? *Geophys. Res. Lett.,* **36,** L12702, doi:10.1029/2009GL038710.

Wunsch, C., and R. Ferrari, 2004: Vertical mixing, energy, and the general circulation of the oceans. *Annu. Rev. Fluid Mech.,* **36,** 281–314.